Mon. Not. R. Astron. Soc. **000**, 1–8 (2007) Printed 25 July 2007 (MN LATEX style file v2.2)

Mapping on the HEALPix grid

Mark R. Calabretta[1] and Boudewijn F. Roukema[2]
[1]*Australia Telescope National Facility, PO Box 76, Epping, NSW 1710, Australia*
[2]*Toruń Centre for Astronomy, N. Copernicus University, ul. Gagarina 11, PL-87-100 Toruń, Poland*

Revised draft for acceptance by MNRAS 2007 July 25

ABSTRACT
The natural spherical projection associated with the Hierarchical Equal Area and isoLatitude Pixelisation, *HEALPix*, is described and shown to be one of a hybrid class that combines the cylindrical equal-area and Collignon projections, not previously documented in the cartographic literature. Projection equations are derived for the class in general and are used to investigate its properties. It is shown that the HEALPix projection suggests a simple method (a) of storing, and (b) visualising data sampled on the grid of the HEALPix pixelisation, and also suggests an extension of the pixelisation that is better suited for these purposes. Potentially useful properties of other members of the class are described, and new triangular and hexagonal pixelisations are constructed from them. Finally, the standard formalism is defined for representing the celestial coordinate system for any member of the class in the FITS data format.

Key words: astronomical data bases: miscellaneous – cosmic microwave background – cosmology: observations – methods: data analysis, statistical – techniques: image processing

1 INTRODUCTION

The Hierarchical Equal Area and isoLatitude Pixelisation, *HEALPix* (Górski et al. 1999, 2005), offers a scheme for distributing $12N^2 (N \in \mathbb{N})$ points as uniformly as possible over the surface of the unit sphere subject to the constraint that the points lie on a relatively small number $(4N - 1)$ of parallels of latitude and are equispaced in longitude on each of these parallels. These properties were chosen to optimise spherical harmonic analysis and other computations performed on the sphere.

In fact, HEALPix goes further than simply defining a distribution of points; it also specifies the boundary between adjacent points and does so in such a way that each occupies the same area. Thus HEALPix is described as an *equal area pixelisation*. Pixels at the same absolute value of the latitude have the same shape in the equatorial region, though pixel shape differs between latitudes, and with longitude in the polar regions. The boundaries for $N = 1$ define the 12 *base-resolution pixels* and higher-order pixelisations are defined by their regular subdivision. Note, however, that although they are four-sided, HEALPix pixels are not spherical quadrilaterals because their edges are not great circle arcs.

HEALPix was originally described purely with reference to the sphere, the data itself being stored as a one-dimensional array in a FITS binary table (Cotton, Tody & Pence 1995) with either *ring* or *nested* organisation, the former being suited for spherical harmonic analysis and the latter for nearest-neighbour searches. For visualisation purposes the software that implements HEALPix (Górski et al. 1997) offers a choice of four conventional projection types onto which HEALPix data may be regridded.

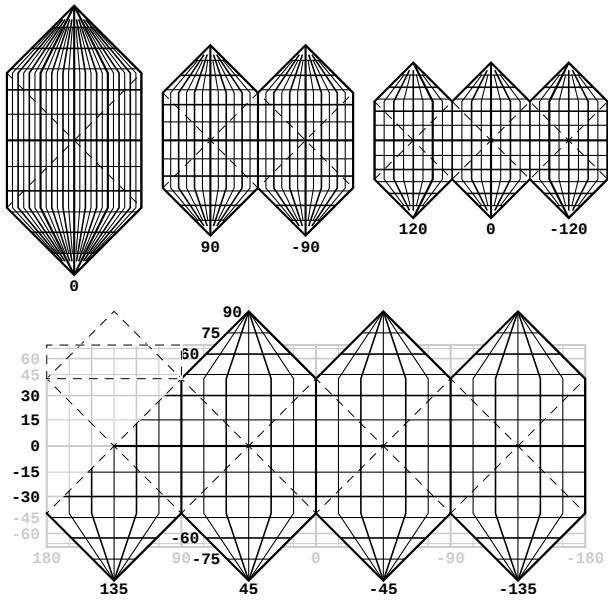

Figure 1. The HEALPix class of projections for $H = 1, 2, 3$ rescaled to unit area (top), and the nominative case with $H = 4$ (bottom) at $\times 4$ the areal scale and with the top left-hand corner of the graticule "cut away" to reveal the underlying cylindrical equal-area projection in the equatorial region. Facets are shown as dashed diamonds.

The mathematics underlying HEALPix is based on mapping each of the twelve base-resolution pixels onto a $[0, 1] \times [0, 1]$ unit square, and this was always an essential feature implemented in the

HEALPix software. Roukema & Lew (2004) have re-derived the pertinent equations and present a diagram showing a projection of the whole sphere (hereinafter the *HEALPix projection*) in which the base-resolution pixels, and consequently the pixels of all higher-order pixelisations, are projected as diamonds (i.e. squares rotated by 45°). These equations may readily be synthesised into those of an equal area projection of the whole sphere.

The HEALPix projection is a combination of a cylindrical equal-area projection in the equatorial region and an interrupted Collignon projection in the polar regions (Collignon 1865; Tissot 1881; Lutque & Matarazzo 2004). This hybrid does not appear to have been documented previously in cartography texts and could not be located in a web search; in particular, it is absent from Snyder's (1993) review of the history of cartography. Illinois State University's MicroCAM web site presents a catalogue of 320 map projections produced by a member of the International Cartographic Association's Commission on Map Projections (Anderson 2003); none bear an obvious resemblance. Of these, the equal-area quadcube may be dissected and rearranged to produce something with a similar boundary but it is a distinctly different projection. The stated intention of this web site is to present as complete a collection as possible of historical, published map projections.

This work will show that the HEALPix projection is one of the more important members of an infinite class of projections parameterised by $H \in \mathbb{N}$ and will derive the projection equations for the class. In particular, the HEALPix projection (i.e. with $H = 4$) suggests a simple way of storing HEALPix data on a two-dimensional square grid as used in conventional imaging and mapping, and also suggests an extension of the HEALPix pixelisation that is better suited to this. The HEALPix projections with $H = 3$, and 6 are also shown to be special, their properties will be discussed, and new hexagonal and triangular pixelisations constructed from them.

The related issues of representing celestial coordinates in the HEALPix projection are also considered in relation to image data storage in FITS (Hanisch et al. 2001).

2 THE HEALPIX PROJECTIONS

Figure 1 shows the first four members ($H = 1, \ldots, 4$) of the HEALPix projections. They may be described as interrupted, equal area, pseudo-cylindrical projections whose defining characteristics are

(i) They are equiareal; regions with equal areas on the sphere have equal areas in the plane of projection.

(ii) Parallels of latitude are projected as horizontal straight lines (interrupted in the polar regions) whence $\partial y/\partial\phi = 0$.

(iii) Parallels are uniformly divided (apart from interruptions).

(iv) The interruptions are defined by stacking equal-area diamonds (hereinafter *facets*) as shown in Fig. 1. The facet that straddles ±180° is split into halves in the graticule,

where we use (ϕ, θ) for longitude and latitude respectively, and (x, y) for Cartesian coordinates in the plane of projection.

These projections correspond to $(N_\phi, N_\theta) \equiv (H, K)$ with $K = 3$ in the genre of isolatitude pixelisations described by Górski et al. (2005). Projections associated with other values of K are readily derived but are only considered peripherally here, though the general equations are cited in Sect. 6. It is interesting to note that the case with $(H, K) = (2, 1)$ is the interrupted, symmetrical form of Collignon's projection as illustrated in Fig. 2. See also Furuti's (2006a) web site which presents geographic outlines.

2.1 HEALPix derivation

In the equatorial regions, the HEALPix projection is based on Lambert's (1772) cylindrical equal area projection whose equations are well known. While Collignon's (1865) derivation of the equations used in the polar region was based on geometry, here we offer a mathematical derivation based on integrating the Jacobian determinant.

In deriving the projection equations, note firstly that for any H the total area occupied by the half-facets in the north polar region is always 1/6 of the total area. Since the projections are equiareal, we equate the area of a spherical cap on the unit sphere, $A = 2\pi(1 - \sin\theta)$, with the corresponding fraction of the total area, $4\pi/6$, to obtain the transition latitude, $\theta_\times$, which is independent of H:

$$\theta_\times = \sin^{-1}(2/3) \approx 41\overset{\circ}{.}8103. \tag{1}$$

2.1.1 Equatorial region

The equatorial region, where $|\theta| \le \theta_\times$, is clearly a cylindrical equal-area projection, i.e. $(x, y) = (\phi, \alpha \sin\theta)$, where α is a constant determined by the requirement that $\theta_\times$ be projected at the vertex of a facet. Since the length of a facet diagonal, e.g. as measured along the equator, is $2\pi/H$, we have $y_\times = \pi/H = \alpha \sin\theta_\times$, whence

$$x = \phi, \tag{2}$$

$$y = \frac{3\pi}{2H} \sin\theta. \tag{3}$$

Because $\partial y/\partial\phi = 0$ for the HEALPix projections the Jacobian determinant reduces to

$$J(\phi, \theta) = \frac{1}{\cos\theta} \frac{\partial x}{\partial\phi} \frac{\partial y}{\partial\theta}. \tag{4}$$

This gives the ratio of an infinitesimal area in the plane of projection to the corresponding area on the sphere. In the equatorial regions it is $3\pi/2H$, a constant, indicative of an equiareal projection. Note that the Jacobian determinant is inversely proportional to H, but the graticules in the top part of Fig. 1 were set to the same areal scale by scaling both x and y by $\sqrt{H}$. Likewise, the remaining graticule, and all others in this paper including Fig. 2, were produced at a consistent areal scale ×4 greater than these first three.

2.1.2 Polar regions

In the polar regions the area north of $\theta (> \theta_\times)$ on the unit sphere is $2\pi(1 - \sin\theta)$ and, noting that the pole is projected at $y = 2\pi/H$, in the plane of projection it is $H(2\pi/H - y)^2$. Equating the ratio of these to the value of the Jacobian determinant obtained for the equatorial region and solving we obtain

$$y = \pm\frac{\pi}{H}(2 - \sigma), \tag{5}$$

where the negative sign is taken for the south polar region, and

$$\sigma = \sqrt{3(1 - |\sin\theta|)} \tag{6}$$

is the ratio of the distance of the pole from the parallel of θ to that of the pole from the parallel of $\theta_\times$.

The equation for x may be obtained readily by integrating Eq. (4) with $\partial y/\partial\theta$ from Eqs. (5) & (6) to produce $x = \sigma\phi + C$, where C is the constant of integration, thus indicating that the parallels are uniformly divided. It is instructive also to consider a geometrical argument; the area of any triangle in the (x, y) plane with

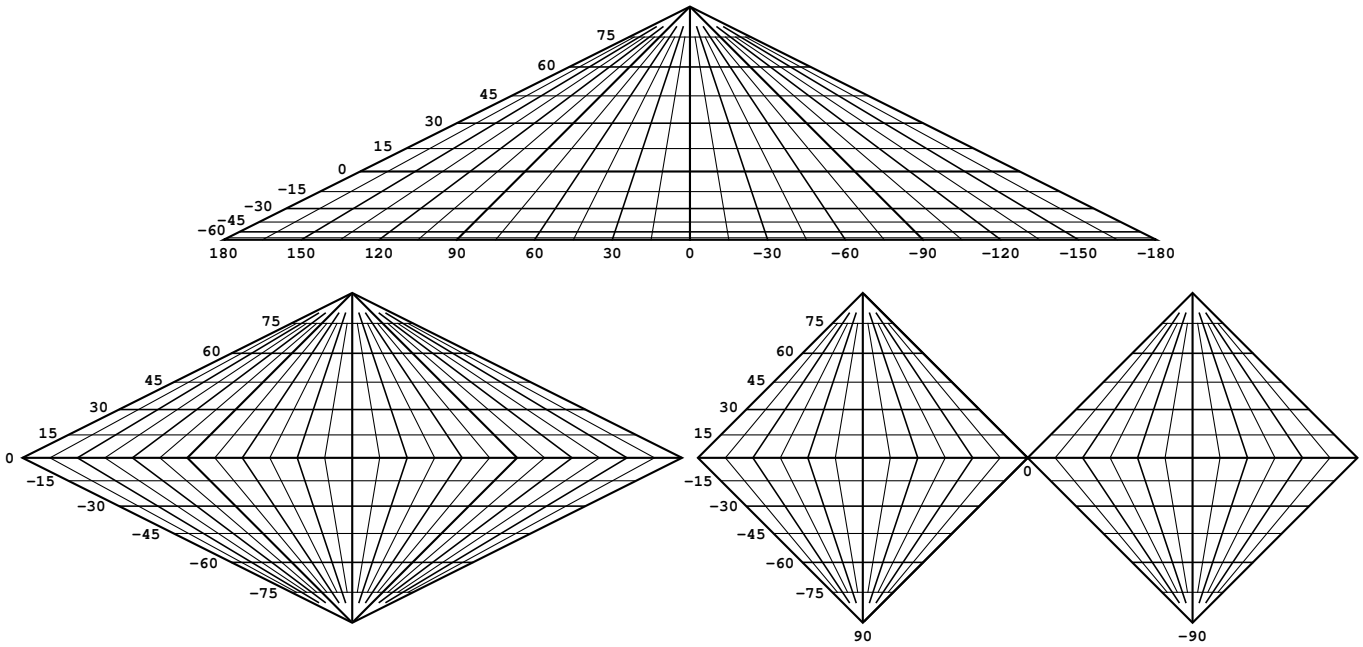

Figure 2. Édouard Collignon's (1865) projections at equi-areal scale: (top) Collignon's projection of the sphere in an isoceles triangle; (bottom left) the northern hemisphere folded about the equator into the south to create a rhombus, rescaling $\times\frac{1}{2}$ in longitude (or $\times\frac{1}{\sqrt{2}}$ and in latitude $\times\sqrt{2}$ to preserve the areal scale) would produce the HEALPix projection with $(H, K) = (1, 1)$; (bottom right) the rhombic case interrupted along the prime meridian and recentred to map each hemisphere onto a square - this corresponds to the HEALPix projection with $(H, K) = (2, 1)$. These and the remaining graticules in this paper are shown at the same areal scale as the bottom panel of Fig. 1 ($H = 4$ case).

its apex at the pole and base along a given parallel of latitude depends only on the change in x between its base vertices and not on their location. Since the projection is equiareal, x must therefore vary linearly with ϕ.

Applying the interruptions to the parallels (this in fact could be omitted or done in other ways to produce different projection types) we have

$$x = \phi_c + (\phi - \phi_c)\,\sigma, \tag{7}$$

where

$$\phi_c = -\pi + \left(2\left\lfloor \frac{(\phi+\pi)H}{2\pi} \right\rfloor + 1\right)\frac{\pi}{H} \tag{8}$$

is the native longitude in the middle of a polar facet and $\lfloor u \rfloor$, the *floor* function, gives the largest integer $\leq u$.

2.2 Properties

The most important feature of the HEALPix projections, indeed the underlying rationale for the HEALPix pixelisation, is that they are equiareal with squared boundaries and straight parallels. Thus they may be completely inscribed by diamonds of equal area, the minimum number of which is $3H$ (the facets). Each facet is subject to further subdivision by N^2 smaller equal-sized diamonds that are identified as *pixels* (picture elements); their centre positions in (ϕ, θ) may be computed readily for any (H, N) from the inverse of the above projection equations as are cited in Sect. 6. As explained by Górski et al. (2005), it is significant for spherical harmonic analysis that the pixel centres lie on a relatively small number of parallels of latitude, and that the facets may be subdivided hierarchically.

Of course a pixelisation may be constructed similarly from a cylindrical equal-area projection, but the HEALPix projections are much less distorted in the polar regions than any such projection. Consequently the HEALPix pixels are truer in shape when projected onto the sphere and their centres are more uniformly distributed. As shown by the dashed lines in the upper-left corner of Fig. 1, the equivalent portion of the underlying cylindrical projection, being severely squashed at the pole, is stretched upwards to twice its height and brought to a point; the pole itself is thereby projected as H points rather than a line. However, this is gained at the cost of introducing $H - 1$ interruptions which should properly be considered as extreme distortions, though of little consequence for the pixelisation.

Evaluating the partial derivatives we find

$$\left(\frac{\partial x}{\partial \phi}, \frac{\partial y}{\partial \theta}\right) = \begin{cases} \left(1,\ \frac{3\pi}{2H}\cos\theta\right) & \ldots \text{equatorial,} \\ \left(\sigma,\ \frac{3\pi}{2H}\frac{\cos\theta}{\sigma}\right) & \ldots \text{polar,} \end{cases} \tag{9}$$

which shows that in the polar regions x is scaled directly, and y is scaled inversely by $\sigma = \sigma(\theta)$ in order for the Jacobian determinant to maintain constancy.

To get some idea of the relative degree of distortion between members of the class, consider first from Eqs. (3) & (5) that y scales as $1/H$ for any θ, while x is independent of H except for defining the interruptions. Hence the relative spacing of parallels between the equator and poles is independent of H, as is evident in Fig. 1, and the distortion is determined solely by the relative $y : x$ scaling. Thus the $H > 1$ projections may be considered to be composed of H rescaled $H = 1$ projections in sequence.

A spherical projection is *conformal* or *orthomorphic* (true shape) at points where the meridians and parallels are orthogonal and equiscaled. The general equations of the cylindrical equal area projection expressed in terms of the conformal or *standard* latitude, $\theta_\circ$, are $(x, y) = (\phi, \sin\theta/\cos^2\theta_\circ)$ (e.g. see Sect. 5.2.2 of Calabretta & Greisen 2002), whence from Eq. (3)

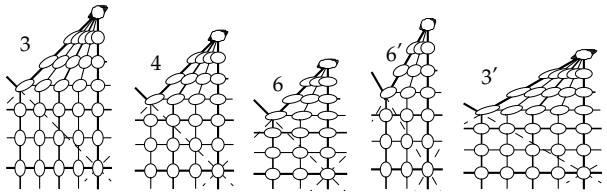

Figure 3. Tissot indicatrices on a 15° graticule for a representative portion of the HEALPix projections with $H = 3, 4$ & 6 at consistent areal scale. The rescaled $H = 6$ & 3 projections associated with the triangular and hexagonal pixelisations discussed in Sects. 4.1 and 4.2 are also shown at the same areal scale. Thus all indicatrices have the same area.

$$\theta_\circ = \cos^{-1}\sqrt{\frac{2H}{3\pi}}. \tag{10}$$

For $H = 1, 2, 3, 4$ this is $(63°, 49°, 37°, 23°)$; the first two of these exceed $\theta_\times$ and hence are inadmissible, and $\theta_\circ$ is undefined for higher values of H. Since the latitude that halves the area of the equatorial region is $\sin^{-1}(1/3) = 19.^\circ5$, independent of H, this suggests that the projection with $H = 4$ is the least distorted in the equatorial regions.

Looking at it another way, the requirement for equiscaling in x and y where the meridians and parallels are orthogonal, i.e. everywhere in the equatorial region, and along the centreline in the polar half-facets, is

$$\frac{1}{\cos\theta}\frac{\partial x}{\partial\phi} = \frac{\partial y}{\partial\theta}. \tag{11}$$

Substituting Eq. (9) gives

$$H_\circ = \begin{cases} \frac{3\pi}{2}\cos^2\theta & \ldots \text{ equatorial,} \\ \frac{\pi}{2}(1 + |\sin\theta|) & \ldots \text{ polar, centreline,} \end{cases} \tag{12}$$

whence $H_\circ = (4.7, 4.4, 3.5, 2.6, 2.7, 2.9, 3.1, 3.1)$ for $\theta = (0, 15°, 30°, \theta_\times, 45°, 60°, 75°, 90°)$. Thus $H = 4$ is a good all-over compromise but for $|\theta| > 30°$, the latitude that halves the hemisphere by area, $H = 3$ would appear to be better on this basis.

The nature of the projective distortion in the region where meridians and parallels are not orthogonal is more complicated and is best illustrated by means of Tissot's indicatrix (e.g. Snyder 1993; or Furuti 2006b). This is the projection, greatly magnified, of an infinitesimal circle on the sphere, as in Fig. 3. In the polar regions the projection of the facets onto the sphere (i.e. the base-resolution pixels) meet at the pole at $360°/H$. For $H = 4$ this is 90° which accords with the angle in the plane of all HEALPix projections. Thus it might seem that $H = 4$ should be least distorted in the neighbourhood of the pole. However, this argument is somewhat misleading; on the sphere the angle between meridians and parallels along the edges of the polar half-facets is always 90°, while in the plane of projection it is always 45°. Tissot's indicatrix shows that $H = 3$ is actually less distorted near the pole.

Tissot's indicatrix also indirectly describes the deformation of the HEALPix pixels themselves. On the sphere the indicatrices are all circles of the same size, whereas on the plane the pixels are all same-sized squares. If the projected Tissot ellipse at the centre of a pixel was rescaled into a circle by compressing its major axis while expanding its minor axis so as to preserve area then the square pixel boundary would become a parallelogram, representative, to first order, of the pixel's shape on the sphere.

Recently Goldberg & Gott (2006) have developed global-average distortion measures for isotropy, I, and area, A, that depend on the map projection metric ($I = 0$ for conformal projections and $A = 0$ for equiareal projections), and also the larger-scale measures of flexion (or bending), F, and skewness (or lopsidedness), S, which are based on the derivatives of the metric. They combine these with the global measure of distance error, D, developed by Gott et al. (2006), with a contribution from boundary discontinuities, B, to derive an overall distortion measure for the projection, Σ_ϵ. The authors kindly provide a code, usable in either IDL® (Interactive Data Language) or GDL (GNU Data Language), to allow others to compute these measures via a Monte Carlo analysis and we have applied it to the HEALPix projection. Results are presented in Table 1 for a variety of parameters H and K and additional y-scaling, as for the triangular and hexagonal pixelisations discussed in Sects. 4.1 and 4.2.

Table 1. Isotropy, area, flexion, skewness, distance and boundary distortion measures for the HEALPix projection, and the overall distortion measure Σ_ϵ, for a selection of H, K and y-rescaling. Measures that equal or improve upon (i.e. are less than) those of the $(H, K) = (4, 3)$ projection are shown in bold. The measures are also computed separately for the equatorial ($|\theta| \leq 30°$) and polar regions for the (3, 3) and (4, 3) projections (italics).

H , K	$y_{\rm scl}$	I	A	F	S	D	B	Σ_ϵ
1 , 1	1	1.17	0	0.70	0.74	**0.38**	**0.25**	9.68
2 , 1	1	0.65	0	0.56	0.48	0.48	**0.50**	**8.19**
3 , 1	1	0.60	0	**0.47**	0.39	0.55	0.75	12.81
2 , 2	1	0.50	0	0.58	0.42	**0.41**	**0.42**	**6.19**
3 , 2	1	0.39	0	**0.49**	0.31	0.45	**0.58**	**7.90**
4 , 2	1	0.49	0	**0.43**	**0.27**	0.50	0.75	11.82
5 , 2	1	0.65	0	**0.37**	**0.25**	0.54	0.92	17.02
2 , 3	1	0.72	0	0.66	0.48	**0.38**	**0.38**	**6.76**
3 , 3	1	0.42	0	0.57	0.33	**0.40**	**0.52**	**6.85**
		0.37	*0*	*0.29*	*0.12*	*0.42*	*0.52*	*Equ.*
		0.45	*0*	*0.86*	*0.53*	*0.54*	*0.52*	*Pol.*
4 , 3	1	**0.36**	0	**0.51**	**0.27**	**0.44**	**0.65**	**9.09**
		0.11	*0*	*0.28*	*0.10*	*0.43*	*0.65*	*Equ.*
		0.50	*0*	*0.75*	*0.45*	*0.57*	*0.65*	*Pol.*
5 , 3	1	0.46	0	**0.47**	**0.26**	0.47	0.79	12.52
6 , 3	1	0.60	0	**0.44**	**0.26**	0.50	0.92	16.82
7 , 3	1	0.73	0	**0.40**	**0.25**	0.53	1.05	21.78
3 , 4	1	0.56	0	0.64	0.37	**0.38**	**0.48**	**6.99**
4 , 4	1	0.40	0	0.58	0.30	**0.41**	**0.60**	**8.18**
5 , 4	1	0.39	0	0.54	**0.27**	**0.43**	0.71	10.50
6 , 4	1	0.48	0	**0.50**	**0.26**	0.46	0.83	13.60
6 , 2	$\sqrt{3}$	**0.31**	0	**0.44**	**0.26**	0.48	1.08	20.94
6 , 3	$\sqrt{3}$	**0.27**	0	0.54	**0.27**	**0.42**	0.92	15.57
6 , 4	$\sqrt{3}$	0.41	0	0.61	0.30	**0.39**	0.83	13.45
3 , 3	$\frac{1}{\sqrt{3}}$	0.59	0	**0.48**	0.31	0.48	**0.52**	**7.59**

For a pixelisation the relevant measures are A, which is zero for all HEALPix projections, and the mean isotropy, I. Like the Tissot indicatrices, I indicates how distorted the pixels are. Of the square (non-rescaled) pixelisations $(H, K) = (4, 3)$ achieves the lowest global mean value of $I = 0.36$ with several others close behind. The associated projection also does well for the other distortion measures, though it falls behind on Σ_ϵ – the overall distortion measure is strongly influenced by B, the total length of boundary discontinuities, which favours smaller H and larger K.

The distortion measures were computed separately for $|\theta| \leq 30°$ and $|\theta| > 30°$ for the (3, 3) and (4, 3) projections, where 30° was chosen in light of the discussion following Eq. 12. As anticipated, the (3, 3) projection does slightly better in the polar region but not

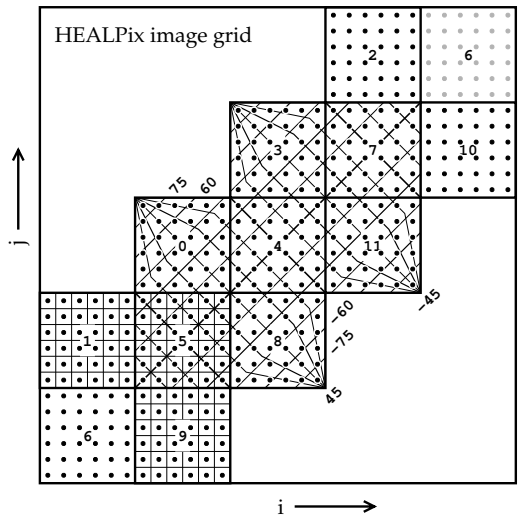

Figure 4. The HEALPix pixelisation for $N = 6$ on the HEALPix projection for $H = 4$ projected with a 45° rotation onto the mapping grid showing the twelve facets with standard numbering. The graticule of the HEALPix projection is shown in the seven facets adjacent to $(\phi, \theta) = (0, 0)$, and those at lower left show the pixel boundaries for $N = 6$ as defined by the HEALPix pixelisation.

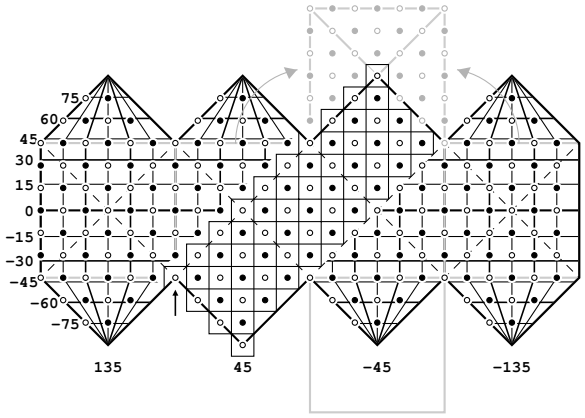

Figure 5. HEALPix double-pixelisation for $N = 3$ on the HEALPix projection with $H = 4$. Filled circles define the regular grid, with interpolated pixels shown as open circles to the east (leftwards) of these. Pixel boundaries are shown in the middle three facets, those of the two additional polar pixels contain a contribution from each of the four adjacent polar facets. One of the eight inside corner pixels with 3/4 area is arrowed. Note the difference between the pixel locations in this figure compared to the $N = 6$ pixelisation in Fig. 4. Also illustrated in grey is the boundary between the faces of the pseudo-quadcube layout of the HEALPix projection, applicable for $(H, K) = (4, 3)$ only.

as well near the equator. However, its global mean isotropy is not far behind the $(4, 3)$ projection and it does better on a number of other measures to produce a lower Σ_ϵ.

With rescaling, the lowest value of I is achieved by $(H, K) = (6, 3)$ with y rescaled by $\sqrt{3}$. Its other distortion measures are also low with the exception of B, the boundary discontinuity, which inflates Σ_ϵ. This projection is the basis of the triangular pixelisation discussed in Sect. 4.1.

3 THE HEALPIX GRID

The base-resolution pixels of the HEALPix pixelisation are projected as diamonds (squares rotated by 45°) on the HEALPix projection with the consequence that the pixel locations fall on a grid with diamond-symmetry.

However, Fig. 4 shows that the diamond grid may trivially be converted to the common square grid used in imaging via a 45° rotation. HEALPix data may thus be displayed directly on the HEALPix projection without regridding and the potential introduction of artefacts. At 48% the resulting image plane is slightly less than half-filled but this is comparable to the figure of 50% for quad-cube projections (O'Neill & Laubscher 1976) which are commonly used in the same type of application as HEALPix. Moreover, being composed of square facets like the quad-cubes, the HEALPix projection also admits the possibility of dissection and storage on a third image axis, such as is implemented for the quad-cubes via the `CUBEFACE` keyword in FITS (Calabretta & Greisen 2002).

Facet number 6 which straddles $\phi = \pm 180°$ may be treated in a number of ways; it may be left split, or the halves may be reconnected in either the lower-left or upper-right corner, or it may be replicated in both.

The *butterfly* projection, the polar variant of Fig. 4 (Stuart Lowe, private comm. 2007), is created by splitting the equatorial facets along the 0° and ±90° meridians, rotating the three resulting *gores* containing facets 0, 1 and 2 by appropriate multiples of 90°, and joining them at the pole to produce an × or "butterfly"-shaped layout. This achieves a 75% filling factor of the enclosing square, now reduced to 4×4 facets.

3.1 HEALPix double-pixelisation

The main drawback with the above technique for storing HEALPix imaging data is that the image is presented at an unusual orientation. However, this may be solved via a simple extension to the HEALPix pixelisation. Figure 5 shows the HEALPix grid with a pixel interposed between every pair of pixels along the parallels of latitude and additional pixels added at the two poles. The total number of pixels in the pixelisation is thereby increased from $12N^2$ to $24N^2 + 2$ without affecting the special properties described by Górski et al. (2005), although requiring a slightly different method of forming the hierarchy and indexing it.

Pixels that fall along the lines where the polar half-facets meet act to "zip" the two edges together. They still have equal area of $4\pi/24N^2$ sr on the sphere, half that of the standard HEALPix pixels, except for the eight pixels in the inside corners. As can be seen in Fig. 5, the latter are incomplete, with only 3/4 of the area, and consequently are three-sided when projected onto the sphere. Collectively their reduced area offsets the contribution from the extra two pixels at the poles.

The pixel index of an interpolated pixel is obtained by adding 0.5 to the HEALPix pixel index (in the ring or nested scheme) of the standard pixel immediately to the west of it (rightwards in Fig. 5). All pixel indexes are then doubled and incremented by unity so that they run from 0 to $24N^2 + 1$ with the first and last at the poles.

The filling factor for this, as of any of the HEALPix projections in the normal orientation, is 75% which exceeds that of the quad-cubes at 50% and is comparable to that of the oft-used Hammer-Aitoff projection at 79%.

Figure 5 shows how the facets of the double-pixelisation may be repartitioned into a configuration that resembles that of a quad-cube projection and by which it becomes amenable to the `CUBEFACE` storage mechanism. However, the resemblance is purely

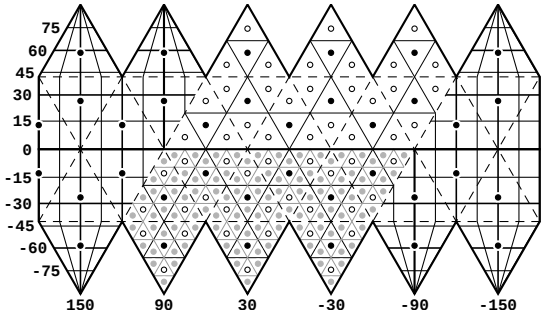

Figure 6. HEALPix projection for $H = 6$ scaled in y by $\sqrt{3}$ whereby the diamond facets become pairs of equilateral triangles - the new base-resolution pixels. These may then be subdivided hierarchically; base-level pixels are shown to the left and right (black circles), the first level of subdivision is at mid-top (thin black), the next at mid-bottom (grey).

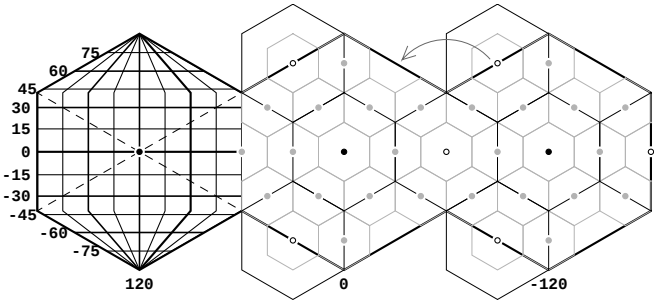

Figure 7. HEALPix projection for $H = 3$ scaled in y by $1/\sqrt{3}$ whereupon it becomes three consecutive hexagons - the new base-resolution pixels; the original diamond facets, now squashed (dashed lines), are superfluous. The graticule of the projection is shown in the left-hand hexagon, whereas those to the right of it show the second (thin black) and third (grey) level of subdivision - each hexagon splits into four non-inscribed hexagons, some of which are shared between two base-resolution pixels as indicated by the arrow.

superficial because the cubeface edges do not match those of a quad-cube projection on the sphere.

4 OTHER PIXELISATIONS

Consider dividing the 360° of circumpolar longitude into integral subdivisions. Of the possible ways of doing this ($1 \times 360°, 2 \times 180°, 3 \times 120°, 4 \times 90°, 5 \times 72°, 6 \times 60°, \ldots$) only the divisions into 3, 4, and 6 correspond to regular polyhedra. The division into $4 \times 90°$ corresponds to the familiar case of HEALPix with $H = 4$ with diamonds tessellated by diamonds.

4.1 Triangular – $H = 6$

However, the division into $6 \times 60°$ suggests a different type of pixelisation in which equilateral triangles are tessellated by equilateral triangles. This pixelisation may be defined by rescaling the HEALPix projection with $H = 6$ by $\sqrt{3}$ in y so that the half-facets become equilateral triangles. Such a linear scaling does not affect the projection's equal area property. What were previously half-facets may now be identified with 36 new, triangular base-resolution pixels that may be subdivided hierarchically as for HEALPix, as depicted in Fig. 6. It is interesting to note that this subdivision is naturally hierarchical – the number of pixels varies exponentially as $36 \times 4^{N-1}$ where N is the hierarchy level. In the $H = 4$ pixelisation the exponential hierarchy must be engineered by doubling N at each level.

The conformal latitude computed for $H = 6$ with this extra y-scaling is $\theta_\circ = 31\overset{\circ}{.}0$, indicating that the projection becomes conformal near the latitude that bisects the hemisphere by area. Applying Eq. (12) with the extra scaling gives $\sqrt{3}H_\circ = (8.2, 7.6, 6.1, 4.5, 4.6, 5.1, 5.3, 5.4)$ for $\theta = (0, 15°, 30°, \theta_\times, 45°, 60°, 75°, 90°)$, again indicating less distortion in the polar regions than $H = 4$. Tissot's indicatrix in Fig. 3 clearly shows that it also does better in the polar zone away from the centreline because the 60° angle along the edge of the polar facets more closely matches the true angle of 90° on the sphere. Overall, this pixelisation performs adequately at low latitudes and does better than the $H = 4$ pixelisations at mid to high latitudes.

This rescaling of the $H = 6$ projection is reminiscent of Tegmark's (1996) icosahedral projection composed of 20 equilateral triangles; the problem of indexing the subdivisions of its triangular facets was solved in the implementation of the corresponding pixelisation. In the present context the isolatitude property is still present but degraded somewhat from the diamond pixelisation of $H = 4$. However, if the pixel centres are moved up or down from the centroid by $\frac{1}{12}$ of the height of the pixel to the point half-way between the base and apex then they fall onto a rectangular grid sampled more frequently in x than y. This provides some of the same benefits as the $H = 4$ double-pixelisation.

Although the displacement is small, there is a possibility that it could introduce statistical biases so the full consequences should be investigated for a particular application. These potential biases may be minimised by making the pixel size sufficiently small, and the fact that the bias between adjacent pairs of pixels is in opposite senses will tend to cancel them over a region encompassing a sufficient number of pixels. It should also be remembered that although the pixel locations *appear* to be at the centre of the pixel boundary in the projection of the diamond, square, and triangular pixelisations this is very much an artefact of the distortions inherent in the projection. Because the y-coordinate varies non-linearly with θ, on the sphere they are actually biased to one side of the pixel. Hence some degree of bias is unavoidable.

4.2 Hexagonal – $H = 3$

The division into $3 \times 120°$ suggests hexagonal base-resolution pixels. Although the familiar "honeycomb" structure shows that it is possible to tile the plane with hexagons, nevertheless there is no bounded tessellation of hexagons by hexagons; that is, no hexagonal region larger than the cell size can be cut out of any honeycomb tessellation without cutting the individual cells. Thus it may seem surprising that a hexagonal pixelisation can be constructed from the HEALPix projection for $H = 3$ with y scaled by $1/\sqrt{3}$. The boundary of this projection, as seen in Fig. 7, is reduced to that of three sequential hexagons and this boundary is then used conceptually as a "pastry-cutter" on a honeycomb tessellation of the right scale. Pixels that are cut can be made whole again by borrowing from adjacent facets, much as the square pixelisation in Fig. 5 does.

The hierarchical pixelisation, somewhat more complicated than for the other cases, is shown in Fig. 7. Like the triangular pixelisation the number of pixels at each level also varies exponentially, as $3 \times 4^{N-1}$. A subdivision of each hexagon into six equilateral triangles is possible but the resulting pixelisation does not satisfy equiscaling in longitude.

Rescaling Eq. (12) gives $H_\circ/\sqrt{3} = (2.7, 2.5, 2.0, 1.5, 1.5,$

1.7, 1.8, 1.8) for $\theta = (0, 15^\circ, 30^\circ, \theta_\times, 45^\circ, 60^\circ, 75^\circ, 90^\circ)$. Thus the rescaled $H = 3$ projection does not achieve conformality at any latitude, it does well close to the equator, but degrades at mid-latitudes. In the polar regions the 30° angle between meridians and parallels along the edge of the facets is further from the ideal of 90° than the 45° angle for the unscaled projections. However, it may be optimal for certain values of the total number of pixels in the pixelisation.

5 $K \neq 3$

The projection equations for general values of K are cited in Sect. 6. The general form of the Jacobian determinant is $J(\phi, \theta) = \pi K/2H$ and the generalisation of Eq. (12) becomes

$$H_\circ = \begin{cases} \frac{\pi K}{2} \cos^2\theta & \ldots \text{ equatorial,} \\ \frac{\pi}{2}(1 + |\sin\theta|) & \ldots \text{ polar, centreline.} \end{cases} \quad (13)$$

This demonstrates that $H_\circ$ is independent of K along the centreline of the polar half-facets and its variation between equator and pole may thus be reduced by choosing K appropriately. For $K = 2$ we find $H_\circ = (3.1, 2.9, 2.4, 2.7, 2.9, 3.1, 3.1)$ for $\theta = (0, 15^\circ, \theta_\times = 30^\circ, 45^\circ, 60^\circ, 75^\circ, 90^\circ)$, and this carries over in particular to the triangular pixelisation. However, it comes at the cost of reducing $\theta_\times$ to 30° thereby increasing the portion of the sphere in the polar half-facets away from the centreline.

6 HPX: HEALPIX IN FITS

In this section the HEALPix projections are described in the same terms as the projections defined in Calabretta & Greisen (2002).

HEALPix projections will be denoted[1] in FITS with algorithm code `HPX` in the `CTYPE`*ia* keywords for the celestial axes. Variable y-scaling as shown in Figs. 6 & 7 may be implemented via `CDELT`*ia*.

As data storage has become much less of an issue in recent years we do not consider it necessary to create an analogue of the `CUBEFACE` keyword to cover `HPX`. However, if HEALPix data in the double-pixelisation is repackaged into the pseudo-quadcube layout shown in Fig. 5 the `CUBEFACE` storage mechanism is applicable for $H = 4$ (only) and will be treated properly by `WCSLIB` (Calabretta 1995).

Since the HEALPix projections are constructed with the origin of the native coordinate system at the reference point, we set

$$(\phi_0, \theta_0)_{\rm HEALPix} = (0, 0). \quad (14)$$

None of the HEALPix projections are scaled true at the reference point in the sense discussed in Sect. 5 of Calabretta & Greisen (2002), nor are the rescaled $H = 3$ & 6 projections, but they are all scaled true in x.

The general form of the projection equations together with their inverses, re-expressed in the form required by FITS with all angles in degrees rather than radians, are now summarised formally.

In the equatorial zone where $|\theta| \leq \theta_\times = \sin^{-1}((K-1)/K)$:

$$x = \phi, \quad (15)$$

$$y = \frac{90^\circ K}{H} \sin\theta, \quad (16)$$

in the polar zones, where $|\theta| > \theta_\times$:

$$x = \phi_{\rm c} + (\phi - \phi_{\rm c})\,\sigma, \quad (17)$$

$$y = \pm\frac{180^\circ}{H}\left(\frac{K+1}{2} - \sigma\right), \quad (18)$$

where the positive sign on y is taken for $\theta > 0$, negative otherwise, and

$$\sigma = \sqrt{K(1 - |\sin\theta|)}, \quad (19)$$

$$\phi_{\rm c} = -180^\circ + \left(2\left\lfloor \frac{(\phi + 180^\circ)H}{360^\circ} + \frac{1-\omega}{2} \right\rfloor + \omega\right)\frac{180^\circ}{H}, \quad (20)$$

$$\omega = \begin{cases} 1 & \ldots \text{ if } K \text{ is odd or } \theta > 0, \\ 0 & \ldots \text{ otherwise.} \end{cases} \quad (21)$$

These equations are readily invertible. In the equatorial zone where $|y| \leq 90^\circ(K-1)/H$:

$$\phi = x, \quad (22)$$

$$\theta = \sin^{-1}\left(\frac{yH}{90^\circ K}\right), \quad (23)$$

in the polar zones, where $|y| > 90^\circ(K-1)/H$:

$$\phi = x_{\rm c} + (x - x_{\rm c})/\sigma, \quad (24)$$

$$\theta = \pm\sin^{-1}\left(1 - \frac{\sigma^2}{K}\right), \quad (25)$$

where the positive sign on θ is taken for $y > 0$, negative otherwise, and

$$\sigma = \frac{K+1}{2} - \frac{|yH|}{180^\circ}, \quad (26)$$

$$x_{\rm c} = -180^\circ + \left(2\left\lfloor \frac{(x + 180^\circ)H}{360^\circ} + \frac{1-\omega}{2} \right\rfloor + \omega\right)\frac{180^\circ}{H}, \quad (27)$$

where $x_{\rm c}$ is the value of x in the middle of a polar facet, as for $\phi_{\rm c}$, and ω is given by Eq. (21).

FITS keywords `PV`i`_1`a and `PV`i`_2`a attached to *latitude* coordinate i will be used to specify H and K with default values 4 and 3 respectively.

`HPX` has been implemented in version 4.0 and later versions of `WCSLIB` which is distributed under the GNU General Public License (GPL).

As of version 4.3, `WCSLIB` includes a utility program that converts 1-D HEALPix pixelisation data stored in a variety of forms in FITS, including ring or nested organisation in a binary table extension, into a 2-D primary image array with `HPX` coordinate representation.

7 SUMMARY

HEALPix projections are constructed as a hybrid of the cylindrical equal area projection in the equatorial regions and the Collignon projection at the poles. The polar vertex of the Collignon projection is cut off at latitude $\sin^{-1}((K-1)/K)$ over the range of longitudes $-180^\circ/H$ to $+180^\circ/H$, and the longitude scale is then stretched by a factor of $H/2$ to make the vertex angle 90°. This right-angled isoceles triangular cap is then replicated and arranged in the prescribed way at the top and bottom of a cylindrical equal area projection truncated at the same latitude. This provides an equi-areal projection which is naturally divisible into diamond (i.e. square) facets.

While in practical cartography Collignon's projection is regarded as little more than a mathematical curiosity, the HEALPix projection makes good use of its property of mapping the sphere

[1] Ratified by the IAU FITS Working Group on 2006/04/26 as an official extension of the FITS WCS standard.

onto squares. That which is awkward for visual representation of the sphere becomes apposite as the basis for constructing an efficient hierarchical pixelisation.

ACKNOWLEDGEMENTS

We wish to thank Carlos Furuti for pointing out the relationship between the HEALPix and Collignon projections and an anonymous referee for a constructive and timely review.

The Australia Telescope is funded by the Commonwealth of Australia for operation as a National Facility managed by CSIRO.

REFERENCES

Anderson P. B., 2003, MicroCAM (Computer Aided Mapping) web site (last updated 2003/Aug) `http://www.ilstu.edu/~microcam/map_projections/`

Calabretta M. R., 1995-2007, `WCSLIB` version 4.2, available from `http://www.atnf.csiro.au/~mcalabre`

Calabretta M. R., Greisen E. W., 2002, A&A, 395, 1077

Collignon É., 1865, Recherches sur la représentation plane de la surface du globe terrestre, Journal de l'École Polytechnique 24, 125

Cotton W. D., Tody D., Pence W. D., 1995, A&AS, 113, 159

Furuti C. A., 1996-2007, `http://www.progonos.com/furuti/`-(a) `MapProj/Normal/ProjPCyl/projPCyl.html#Collignon` (b) `MapProj/Normal/CartProp/Distort/distort.html`

Goldberg D. M., Gott J. R., 2006, Cartographica (accepted), arXiv:astro-ph/0608501

Górski, K. M. et al., 1997-2007, The HEALPix homepage `http://healpix.jpl.nasa.gov`

Górski, K. M., Hivon, E., Wandelt, B. D., 1999, in Proceedings of the MPA/ESO Cosmology Conference "Evolution of Large-Scale Structure", p37, eds. A. J. Banday, R. S. Sheth, and L. Da Costa (PrintPartners Ipskamp, NL) (arXiv:astro-ph/9812350)

Górski K. M., Hivon E., Banday A. J., Wandelt B. D., Hansen F. K., Reinecke M., Bartelmann M., 2005, ApJ, 622, 759 (arXiv:astro-ph/0409513)

Gott J. R., Mugnolo C., Colley W.N. 2006, arXiv:astro-ph/0608500

Hanisch R. J., Farris A., Greisen E. W., Pence W. D., Schlesinger B. M., Teuben P. J., Thompson R. W., Warnock III A., 2001, A&A, 376, 359

Lambert J.H., 1772, Anmerkungen und Zusätze zur Entwerfung der Land und Himmelscharten. In *Beiträge zum Gebrauche der Mathematik und deren Anwendung*, pt. 3, sec. 6. (English translation: Notes and Comments on the Composition of Terrestrial and Celestial Maps, Ann Arbor, University of Michigan 1972)

Luque M., Matarazzo G., 2004, Projection Collignon à méridiens et parallèles rectilignes, `http://melusine.eu.org/syracuse/mluque/mappemonde/doc-collignon/collignon.html`

O'Neill E. M., Laubscher R. E., 1976, Extended Studies of the Quadrilateralized Spherical Cube Earth Data Base, NEPRF Technical Report 3 – 76 (CSC) Computer Sciences Corporation (Silver Springs, Maryland)

Roukema B.F., Lew B., 2004, arXiv:astro-ph/0409533

Snyder J. P., 1993, Flattening the Earth (University of Chicago Press, Chicago and London)

Tegmark M., 1996, ApJ, 470, L81

Tissot A., 1881, Mémoire sur la représentation des surfaces et les projections des cartes géographiques (Gauthier-Villars, Paris)